Shang, Bin; Zhang, Xiaofen; Ji, Ri; Wang, Yanbing; Hu, He; Peng, Bo; Deng, Ziwei

Preparation of colloidal polydopamine/Au hollow spheres for enhanced ultrasound contrast imaging and photothermal therapy

Published in:
Materials Science and Engineering C

DOI:
10.1016/j.msec.2019.110174

Published: 01/01/2020

Document Version
Peer-reviewed accepted author manuscript, also known as Final accepted manuscript or Post-print

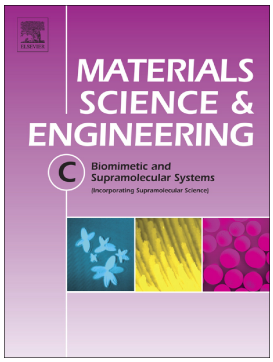

Preparation of colloidal polydopamine/Au hollow spheres for enhanced ultrasound contrast imaging and photothermal therapy

Bin Shang, Xiaofen Zhang, Ri Ji, Yanbing Wang, He Hu, Bo Peng, Ziwei Deng

PII: S0928-4931(18)33169-2

DOI: https://doi.org/10.1016/j.msec.2019.110174

Reference: MSC 110174

To appear in: *Materials Science & Engineering C*

Received date: 16 October 2018

Revised date: 6 September 2019

Accepted date: 6 September 2019

Please cite this article as: B. Shang, X. Zhang, R. Ji, et al., Preparation of colloidal polydopamine/Au hollow spheres for enhanced ultrasound contrast imaging and photothermal therapy, *Materials Science & Engineering C* (2018), https://doi.org/10.1016/j.msec.2019.110174

Preparation of colloidal polydopamine/Au hollow spheres for enhanced ultrasound contrast imaging and photothermal therapy

Bin Shang [a1], Xiaofen Zhang [b1], Ri Ji [c1], Yanbing Wang [a], He Hu [d], Bo Peng [e,*], Ziwei Deng [a,*]

[a] Key Laboratory of Applied Surface and Colloid Chemistry, Ministry of Education, Shaanxi Key Laboratory for Advanced Energy Devices, Shaanxi Engineering Lab for Advanced Energy Technology, School of Materials Science and Engineering, Shaanxi Normal University, Xi'an, 710119, China.

[b] The Key Laboratory of Resource Chemistry of Ministry of Education, Shanghai Key Laboratory of Rare Earth Functional Materials, and Shanghai Municipal Education Committee Key Laboratory of Molecular Imaging Probes and Sensors, Shanghai Normal University, Shanghai 200234, China.

[c] Department of Ultrasound, Ruijin Hospital, Shanghai Jiaotong University School of Medicine, Shanghai, 200025, China.

[d] Department of NanoEngineering, Moores Cancer Center, University of California, San Diego, CA 92093, U.S.A.

[e] Department of Applied Physics, Aalto University, Espoo FI-00076, Finland.

[1] These three authors contributed equally to this work.

Corresponding authors:

* Dr. Bo Peng, E-mail: pengbo006@gmail.com

* Prof. Ziwei Deng, E-mail: zwdeng@snnu.edu.cn

ABSTRACT

Development of functional theranostic platform for systemic contrast-enhanced diagnostic imaging and therapy is of great necessity in nanomedicine. However, synthesizing the biocompatible theranostic agents with enhanced merits in imaging and therapy via a facile and green way is still highly challenged. Here, we report a novel theranostic agent based on colloidal polydopamine/Au (PDA/Au) hollow spheres, which are synthesized with combined use of PDA chemistry and sacrificial template techniques. Colloidal polystyrene (PS) spheres serve as the templates with coatings of a PDA shell and Au nanoparticles in sequence, which are subsequently removed with trichloromethane, giving rise to colloidal PDA/Au hollow spheres. Colloidal PDA/Au hollow spheres exhibit excellent contrast enhancement for ultrasound imaging, and can serve as the near-infrared (NIR) photoabsorbers for the effective photothermal ablation of 4T1 breast cancer cells *in vitro* with minor cytotoxicity to living cells. This method suggests a novel avenue for theranostic treatment in oncology.

Keywords: Polydopamine; Au nanoparticles; Hollow spheres; Ultrasound imaging; Photothermal therapy.

1. Introduction

Recent advances in nanomedicine have prompted the development of multifunctional nanocomposites that have combined diagnostic and therapeutic functions within a single biocompatible platform [1-3]. Taking advantage of their combined physical, chemical, and biological characteristics, multifunctional nanocomposites can be used as the theranostic agents for the multimodal bioimaging and therapy applications. Therefore, tremendous efforts have recently been devoted to develop new synthetic paths towards multifunctional nanocomposites, which are potentially potent to accomplish simultaneous diagnosis and therapy [1, 4].

Recently, there has been growing interest in the combination of ultrasound imaging and photothermal therapy for a better diagnosis in comparison with conventional way to guide and monitor photothermal therapy for cancers [5-7]. In principle, ultrasound imaging is used to identify the location of the tumors [8-11], and the near-infrared (NIR) laser-induced photothermal therapy is subsequently introduced to ablate tumors. Note that the near-infrared (NIR) laser is intently applied for the photothermal treatment, where the absorption of the human tissues is minimal and the penetration is optimal [12]. The combined use of both techniques would provide an economic, convenient, and non-invasive path with multifunction for cancer treatment [5-7, 13]. Although this combined technique can significantly advance the simultaneous imaging and photothermal therapy, the proper theranostic agents are rather scarce. Ultrasound imaging requires materials with hollow structures, and the photothermal therapy demands materials that can efficiently transform light to heat. Mostly, gold nanoshelled-poly (lactic acid) (PLA) micro/nanocapsules have been synthesized and applied as the multifunctional theranostic agents for contrast-enhanced ultrasound imaging guided photothermal therapy [5, 13-15]. Moreover, the CuS nanoparticles deposited-microbubbles, and polypyrrole [16] and

Prussian blue [17] hollow particles have also been developed for this purpose. Despite their success in the ultrasound imaging guided photothermal therapy, their complicated fabrication process and/or the potential poor biocompatibility might hinder their use in practice. Therefore, the development of biocompatible theranostic agents with excellent echogenic response and good photohyperthermia effects through a simple way is emergently desired.

Polydopamine (PDA) is a synthetic analogue of naturally occurring melanin with many striking physicochemical properties, including adhesive, biocompatible and biodegradable, which promise a number of bioapplications in drug delivery, diagnosis and therapy [18-21]. As such, PDA hollow particles are assumed to be a superior candidate for the ultrasound imaging [22]. In addition, very recently, PDA has also been demonstrated with excellent photothermal activity, which is promising for photothermal therapy [23, 24]. Besides, Au nanoparticles have been extensively employed as the contrast agents for enhancing the biomedical imaging [5], as well as the agents for photothermal cancer therapy due to their magnificent optical properties (*e.g.*, the localized surface plasmon resonance absorption, and the scattering ability in NIR region) and their excellent biocompatibility [25-27]. Thus, coupling PDA hollow particles with Au nanoparticles may result in a composite material with enhanced performance in ultrasound imaging guided photothermal therapy. To the best of our knowledge, there are currently no report of a theranostic platform that combines PDA hollow particles with Au nanoparticles for simultaneous ultrasound imaging and enhanced photothermal therapy.

Here, we show a facile synthetic route towards colloidal PDA/Au hollow spheres that are potent for simultaneous ultrasound imaging and photothermal therapy. In this approach, monodisperse colloidal PS spheres as the templates are first coated with a PDA shell through self-polymerization of dopamine in a weakly alkaline aqueous environment and then with Au

nanoparticles via the *in situ* reduction of the Au precursors in the absence of extra reductants or pre-surface modification, finally resulting in PS/PDA/Au core-shell-shell structured composite particles. The loading amount and the size of Au nanoparticles can be controlled by adjusting the concentration of the Au precursor. After the removal of PS templates with trichloromethane, colloidal PDA/Au hollow spheres are yielded. These colloidal PDA/Au hollow spheres are used as the dual-functional theranostic agents for both ultrasound imaging diagnosis and NIR laser induced photothermal ablation therapy. They exhibit a synergetic effect in the theranostic application, holding great potential for *in vivo* cancer diagnosis and therapy in practice.

2. Experimental section

2.1. Materials

All chemicals were of analytic grade and used as received unless otherwise mentioned. Polyvinylpyrrolidone (PVP, MW = 40000 g/mol), tris (hydroxymethyl) aminomethane (Trizma®base, ≥99.8%) and 3-hydroxytyramine hydrochloride (dopamine hydrochloride) were purchased from Sigma-Aldrich. 2,2'-azobisisobutyronitrile (AIBN) was brought from Shanghai Chemical Reagent Co. (China) and was purified by recrystallization in ethanol. Styrene was purchased from Tianjin Tianli Chemical Reagent Co., Ltd. (China) and was distilled to remove the inhibitor in vacuum, and stored at 4 ^{o}C until use. Chloroauric acid hydrated ($HAuCl_4 \cdot 4H_2O$), hydrochloric acid (HCl, 36 wt% in water), trichloromethane and ethanol were supplied by Sinopharm Chemical Reagent Co., Ltd (China). Ultrapure water (>17 MΩ cm^{-1}) was made from a GZY-P10 water system and used throughout the experiments.

2.2. Preparation of polydopamine/Au hollow spheres

First, monodisperse colloidal polystyrene (PS) spheres as the templates were prepared via dispersion polymerization according to our previous works [28-30]. The core–shell structured PS/PDA composite spheres were prepared in the dopamine solution in the presence of the PS spheres. In brief: dopamine aqueous solution (2 mg/mL) was first prepared by dissolving dopamine (200 mg) in a freshly prepared Tris-HCl buffer solution (100 mL, 10 mM and pH 8.5). Then, the PS powder (0.2 g) was dispersed into the dopamine solution aided by sonication. After 24 h of magnetic stirring at room temperature, colloidal PS spheres were coated with PDA shells. Finally, the PS/PDA core-shell composite spheres were separated with a centrifuge and washed with ethanol for several times, and finally dried in vacuum at room temperature for 24 h.

Second, the PS/PDA/Au composite spheres were prepared as follows: a solution consisting of 0.1 wt % of PS/PDA composite spheres was prepared by dispersing a certain amount of PS/PDA powders into water. Subsequently, the desired amounts of $HAuCl_4$ aqueous solution (10 mg/mL) were added into 30 mL particle dispersion. The reaction was magnetically stirred at room temperature for 1 h. The PS/PDA/Au composite spheres were collected by centrifugation, and rinsed with ultrapure water and ethanol for several times.

Finally, these PS/PDA/Au composite spheres were treated with trichloromethane to remove the PS templates. The colloidal PDA/Au hollow spheres were collected by centrifugation, and washed with trichloromethane and ethanol twice. The product was dried in a vacuum oven, and stored in glass vials for further use.

2.3. Characterization

The morphologies of the colloidal spheres were examined with a transmission electron microscope (TEM, JEOL JEM-2100, Japan). Prior to examination, all samples were diluted with ethanol, ultrasonicated at 25 ^{o}C for 10 min, and dried on the carbon-coated copper grids. X-ray photoelectron spectroscopy (XPS) was performed on an AXIS Ultra X-ray photoelectron spectrometer (Kratos Analytical Ltd., UK) equipped with a monochromatized Al K X-ray source (1486.6eV). All binding energies were calibrated by using the containment carbon (C1s =284.6 eV). Powder X-ray diffraction was performed on a DX-2700 X-ray diffractometer equipped with a Cu tube and a diffracted beam curved graphite monochromator operation at 40 kV and 30 mA. Crystal structure identification was carried out by scanning the powders deposited on the glass substrates with a scanning rate of 0.02° (2θ) per second in the range of 10 to 80°. Thermogravimetric analysis (TGA) was performed on the SDT Q600 (TA Instruments. U.S.A.). All dry samples were heated from 25 to 800 ^{o}C at a heating rate of 10 ^{o}C min^{-1} under a nitrogen atmosphere with a flow rate of 50 mL min^{-1}.

2.4. In vitro ultrasound imaging

The *in vitro* ultrasound imaging of colloidal PDA/Au hollow spheres was performed on a Mylab 90 scanner (Esaote Medical Systems, Genova, Italy). Typically, the physiological saline solution with different concentrations of colloidal PDA/Au hollow spheres (0-0.2 mg/mL) was first filled into an Eppendorf tube (2 mL), and then the tube was immerged into a pure water tank. The ultrasound imaging was achieved by using an LA435 linear-array transducer with different frequencies and mechanical indices (MIs). The transducer was coated with ultrasonic coupling

agent to avoid air background. All images and videos were recorded as the digital files for subsequent playback and analysis.

2.5. Cell culture

4T1 breast cancer cells (4T1 cells) were provided by Shanghai Cancer Center & Department of Oncology (China) and cultured in the Dulbecco's Modified Eagle Medium (Hyclone) supplemented with 10% fetal bovine serum (FBS) and penicillin–streptomycin solution (100 UmL^{-1}, 100 μg mL^{-1}, Gibco) at 37 ^{o}C in a humidified atmosphere of 5% CO_2. They were seeded with an equal density in each well in 96-well plates (1×10^4 cells per well) in 100 mL of Dulbecco's Modified Eagle Medium (DMEM) supplemented with 10% fetal bovine serum (FBS) for 24 h at 37 ^{o}C, a humidified atmosphere of 5% CO_2-containing atmosphere, and grown overnight before further studies.

2.6. In vitro cytotoxicity and cell viability evaluation

The *in vitro* cytotoxicity of colloidal PDA/Au hollow spheres against 4T1 breast cancer cells was evaluated by the MTT (3-(4, 5-dimethyl thiazol-2-yl)-2, 5-diphenyl tetrazolium bromide). Specifically, 4T1 cells were seeded in 96-well plates with a density of 1×10^4 cells per well in a standard growth medium and cultured in a humidified atmosphere of 5% CO_2 at 37 ^{o}C for 24 h before the exposure to the above materials. Then, 4T1 cells were incubated in the growth medium containing different concentrations of PDA/Au hollow spheres (10, 20, 50, 100, and 200 μg/mL) for another 24 h. Meanwhile, the wells containing the cell medium only were also prepared as the controls. After the treatment, MTT was chosen as the indicator of the cell viability as determined by the mitochondrial-dependent reduction to formazane. The MTT (5 mg/mL, 20 μL) solution was infused into each well and the plates were incubated for another 4 h

at 37 ^{o}C in a humidified atmosphere of 5% CO_2. The supernatant was discarded, following by the addition of dimethyl sulfoxide (DMSO, 150μL/well) to completely dissolve the formazan crystals. The absorbance of each well was measured using a Multiskan MK3 enzyme-linked immunosorbent assay reader.

2.7. Measurement of photothermal performance

For measuring the photothermal conversion performance of colloidal PDA/Au hollow spheres, 2 mL aqueous dispersion of hollow spheres at different concentrations (50-300 μg/mL) were added into a quartz cuvette and were irradiated under an 808 nm NIR laser at a power density of 1 W/cm^2 for 15 min. The thermal imager (FLIR A300) equipped with a thermal imaging camera was used to monitor the real time temperature.

2.8. Photothermal cytotoxicity

Photothermal cytotoxicity of colloidal PDA/Au hollow spheres was evaluated with 4T1 breast cancer cells. To assess the photothermal effect on 4T1 cells, 4T1 cells were incubated at 37 ^{o}C in a humidified atmosphere of 5% CO_2 containing different concentrations of colloidal PDA/Au hollow spheres (0, 25, 50, 100,150, and 200 μg/mL) for 1 h. Eventually, the whole system was exposed to an 808 nm NIR laser at a power density of 1 W/cm^2 for 10 min and incubated for another 1 h. The viability of cell was evaluated by an MTT assay.

3. Results and discussion

This synthesis combines mussel-inspired polydopamine chemistry and sequential sacrificial template techniques, as illustrated in Fig. 1a. Colloidal PS spheres were chosen as the templates because of their advantageous features, including commercially available, monodisperse, size tunable, diverse surface groups, bio-inert, and etc. [30]. TEM images in Fig. 1b confirmed that the original PS spheres were fairly uniform both in size and spherical morphology with a mean diameter of 1.71 μm and a low polydispersity of 0.75% (by averaging 100 particles in the TEM micrographs, see Fig. S1a). Moreover, PS spheres were observed with smooth surfaces in a high magnification TEM image (see the inset in Fig. 1b).

Although monodisperse PS spheres can serve as the templates, they are difficult to directly integrate inorganic components onto their surfaces because of lack of functional groups, resulting in the limitation on construction of organic-inorganic composite materials. Otherwise, surface activation or introduction of linkers is required [31]. Nevertheless, mussel-inspired PDA chemistry circumvents these problems because it offers a general way to coat PDA onto various surfaces regardless of the morphology and the chemistry of the surfaces. On the other hand, the as-prepared PDA coatings can serve as a versatile platform for diverse secondary surface-mediated reactions, succeeding in introducing a range of functional materials [18-20, 28, 30]. Surface modification of colloidal PS spheres with PDA was illustrated in Figure 1a. In comparison with the pristine PS spheres (see Fig. 1b), the PDA coatings do not have a significant influence on the morphologies of the PS spheres, indicating a homogeneous PDA coating formed. However, both the average size and surface roughness of the PS/PDA composite spheres increased (see Fig. 1c). The average diameter of the colloidal PS/PDA composite spheres is 1.85 μm, indicating that the thickness of the PDA shell is about 70 nm. The polydispersity of the

PS/PDA composite spheres is 1.35% (see Fig. S1b), further verifying the formation of homogeneous PDA shells.

Mussel-inspired PDA coatings can serve as a multifunctional layer, allowing for the introduction of a rich variety of secondary reactions because of their inherent active catechol and amine groups [28-30, 32]. As such, Au nanoparticles can be *in situ* formed onto the surface of the colloidal PS/PDA composite spheres via a so-called polydopamine-assisted electroless metallization process [19, 28, 32-34], as illustrated in Fig. 1a. It is worth pointing out that the polydopamine-assisted electroless metallization is a simple and environmentally friendly approach to prepare PDA/metal nanocomposites. The detailed reaction mechanism is described as follows: The apparent reductive capacity of PDA is ascribed to those catechol groups present on their surface. Those catechol groups can release electrons when oxidized into the corresponding quinone groups, which enable to trigger the reduction processes of noble metal ions into the corresponding metals [18, 35]. In this process, the PDA shells can serve not only as the linker, coupling PS with Au nanoparticles, but also as the reductant, *in situ* reducing the $AuCl_4^-$ ions into metallic Au nanoparticles under mild reaction conditions. Neither additional reductants, nor toxic reagents, nor intricate instruments were required during this process. The decorated Au nanoparticles were observed by TEM, as shown in Fig. 1d. In comparison with the colloidal PS/PDA composite spheres (Fig. 1c), PS/PDA/Au composite spheres have relative rough surfaces, and a huge contrast between PS/PDA and Au nanoparticles can be observed. The Au nanoparticles were homogeneously distributed over the surfaces of the colloidal PS/PDA composite spheres with an average size of 27.7 nm as shown in Fig. 1d and Fig. S1c.

To synthesize hollow PDA/Au composite spheres, the PS cores were selectively removed with its good solvent, *i.e.*, trichloromethane, as schematically illustrated in Fig. 1a. After the treatment

with trichloromethane, the color of the cores became lighter than before the treatment as comparing with Fig. 1d and e. The hollow structures were verified by using elemental mapping analysis as shown in Fig. 1f. The O element was only present within the shell of the particles, which was solely contributed from PDA rather than PS. Notably, the removal of the PS cores did not affect the shell structures of the PDA/Au particles, and no Au nanoparticles were observed to fall off from or aggregate on the surfaces of the PDA shells, indicating the strong coordination between the catechol groups and Au nanoparticles. The elemental mapping results in Fig. 1f were consistent with the results from TEM.

X-ray photoelectron spectroscopy (XPS) has been employed to analyze the surface chemical composition of the samples. As shown in Fig. 1g, the strong C1s signal peak accompanying with the weak characteristic signals of O1s and N1s peaks can be observed for the spectrum of the PS spheres. After coating with PDA, the intensities of both O1s and N1s peaks were extensively enhanced. It is also found that the surface O/C mole ratio of the PS/PDA composite spheres was higher than that of the PS spheres, which was ascribed to the richer oxygen gradient of the PDA than PS. After the decoration of the Au nanoparticles, besides C1s, N1s and O1s peaks, the new peaks including Au4d ($Au4d_{5/2}$, $Au4d_{3/2}$) and Au4f appear. This is the strong evidence of the emergence of the Au nanoparticles. Although the PS spheres are removed by trichloromethane, the XPS spectrum of the colloidal PDA/Au hollow spheres resembled to that of the PS/PDA/Au composite spheres. This is probably because XPS can only detect about few tens of nanometers deep from the surfaces [36]. In addition, X-ray diffraction (XRD) was introduced to analyze the crystal structure of the Au nanoparticles formed. As shown in Fig. 1h, the broad peaks at 2θ angle of 10° and 30° were attributed to amorphous polymers (*e.g.*, PS and PDA). After the decoration of the Au nanoparticles, the new peaks appeared at 38.1, 44.3, 64.5, and 77.5°

correspond to the reflections of the (111), (200), (220), and (311) crystalline planes of the face-centered cubic (*fcc*) structured Au, respectively. All results evidence the successful preparation of colloidal PDA/Au hollow spheres.

In this process, the size and loading content of the Au nanoparticles on the surfaces of the PDA hollow spheres can be easily tunable by varying the content of the Au precursor-$HAuCl_4$. As observed in Fig. 2a-c, the average sizes and loading densities of the Au nanoparticles were increased with increasing the content of $HAuCl_4$. The average sizes of the Au nanoparticles (see Fig. 2a, b, and c, denoted as PDA/Au-i, PDA/Au-ii, and PDA/Au-iii, respectively) were increased from 13 to 29 nm (see Fig. 2d, e, and f) with concentrations of $HAuCl_4$ increased from 0.10 to 0.33 mg/mL, respectively. Even though at a high concentration of $HAuCl_4$, no free Au nanoparticles were observed, further indicating the excellent binding ability of the PDA coatings to Au nanoparticles.

Additionally, XRD was performed to ascertain the grain size of the Au nanoparticles. As shown in Fig. 2g, there are broad peaks at 2θ angle of 10° and 30°, which are attributed to the PDA polymer [33]. Additionally, the strongest characteristic reflection (111) of the Au nanoparticles can be used to calculate the average crystallite size according to the Debye–Scherrer equation. The average grain size increases from 14 to 31 nm with increasing the concentration of $HAuCl_4$ from 0.10 to 0.33 mol/mL, which exhibited a good agreement with the results from TEM in Fig. 2a-c. This also indicates that the individual Au nanoparticles are single crystal. Then, to quantitatively determine the loading amount of the Au nanoparticles, thermogravimetric analysis (TGA) was applied. As the results shown in Fig. 2h and Fig. S2, the weight loss increased as decreasing the content of the $HAuCl_4$ used. In the other word, more Au

nanoparticles were loaded with increasing the concentration of $HAuCl_4$. The final residue weights corresponding to PDA/Au-i, PDA/Au-ii, and PDA/Au-iii were 49.15%, 53.48% and 57.67%, respectively (see Fig. 2h).

To explore the applications of the colloidal PDA/Au hollow spheres as ultrasound imaging contrast agent, their ultrasound contrasting efficiency was systematically evaluated in a physiological saline solution. The *in vitro* ultrasound imaging of the colloidal PDA/Au hollow spheres was investigated by using Mylab 90 scanner systems. Based on previous studies [37-39], the MI and constant frequency were fixed at 0.060 and 9 MHz, respectively, and the ultrasound imaging of PDA/Au-i, ii, iii were investigated, as shown in Fig. 3. As the concentration of the hollow spheres ranged from 0.04 to 0.20 mg/mL, the intensity of the ultrasound signals increased for all three samples with the concentration from 0.04 to 0.10 mg/mL, but slightly dropped off at the highest concentration of 0.20 mg/mL, which may be attributed to the high concentration induced aggregation. The optimal ultrasound images were found by using PDA/Au- ii and iii at the concentrations of 0.06~0.10 mg/mL. Furthermore, it was observed that the ultrasound signals were enhanced with increasing the loading of the Au nanoparticles. This result indicated that the presence of the Au nanoparticles on the shell of the hollow spheres can boost the acoustic impedance and enhance the detectable scattering, resulting in intensified scattering signals and consequently ultrasound imaging [5]. Thus, these colloidal PDA/Au hollow spheres demonstrated great potential as efficient contrast agents for ultrasound imaging.

Next, the NIR absorption and photothermal conversion efficiencies of the colloidal PDA/Au hollow spheres were evaluated. As shown in Fig. 4a, the colloidal PDA hollow spheres exhibited a broad absorption ranging from visible to NIR regions. After coating with Au nanoparticles, the localized surface Plasmon resonance (LSPR) peaks of the colloidal PDA/Au hollow spheres

located at 570 nm. Moreover, colloidal PDA/Au hollow spheres showed the enhanced absorbance at the long wavelength (600-1000 nm) region in comparison with that of colloidal PDA hollow spheres, suggesting that these colloidal PDA/Au hollow spheres could be suitable for photothermal therapy with laser in the NIR region.

Subsequently, we further studied the photothermal effect of the hollow spheres induced by NIR irradiation. The colloidal PDA and PDA/Au hollow spheres were first dispersed in phosphate-buffered saline (PBS), and were then irradiated with an 808 nm NIR laser at a power density of 1 W/cm^2 for 900 s. The pure PBS was used as a control. Although the temperatures in samples increased with the prolonged NIR irradiation time, the elevation ratio of the temperature in each samples followed the order: PDA/Au > PDA > control (Fig.4b). This order indicated that the Au nanoparticles enhanced the photothermal conversion ability of colloidal PDA hollow spheres. Furthermore, the colloidal PDA/Au hollow spheres displayed a concentration-dependent photothermal property, as demonstrated in Fig. 4c. With the increase of PDA/Au hollow spheres in PBS solution, the solution temperature increased with increasing the concentration of the colloidal PDA/Au hollow spheres. Then, we further measured the photothermal conversion efficiency (η) of the colloidal PDA/Au hollow spheres. Upon turning on the NIR laser irradiation for 900 s, the colloidal PDA/Au hollow spheres (at the concentration: 200 μg/mL) raised the temperature by 13.5 ^{o}C. The temperature then gradually decreased back to original point in about 600 s. As exhibited in the inset of Fig. 4d, the η value of the PDA/Au hollow spheres was calculated to be 19.88% [23, 40-42]. Our results clearly demonstrated that those PDA/Au hollow spheres displayed good photothermal properties, which make them promising as a photothermal agent.

Prior to putting colloidal PDA/Au hollow spheres into application, their cytotoxicity was evaluated by using MTT assay. As demonstrated in Fig. S3 and Fig. 5c, the colloidal PDA/Au hollow spheres did not show a significant cytotoxicity against cells. Even increasing the concentration of the hollow spheres to 200 μg/mL, 88.9% of the cells were viable after 24 h incubation. This suggests that colloidal PDA/Au hollow spheres had a minor cytotoxicity to living cells.

Based on the superior photothermal activity and biocompatibility of the colloidal PDA/Au hollow spheres, we further explore their usage in photothermal ablating cancer cells *in vitro*. To achieve this, 4T1 breast cancer cells (4T1 cells) were selected as the model. The 4T1 cells were incubated with colloidal PDA/Au hollow spheres for 1 h at 37 ^{o}C and then irradiated by 808 nm NIR laser at 1 W/cm^2 for 10 min. Before irradiation, calcein acetoxymethyl ester (calcein-AM)/propidium iodide (PI) were employed to stain the live (green) and dead cells (red), respectively. In this way, the viability of the cells can be directly detected by confocal laser scanning microscopy (CLSM). As seen from Fig. 5a and b, while the 4T1 cells showed the intense green fluorescence of calcein-AM before irradiation, illustrating the survival of the major 4T1 cells, the cells were looked reddish after irradiation, suggesting the high efficacy of the colloidal PDA/Au hollow spheres in killing cancer cells in aid of NIR laser irradiation. Further, we also quantitatively explored the impact of the concentration of the hollow spheres on photothermal treatment of the cells. As displayed in Fig. 5c, the concentration of the hollow spheres had a minor impact on the cell viability in the absence of the irradiation. Thanks to the irradiation, the cell viability was significantly decreased as shown in Fig. 5d. Increasing the concentration of the hollow spheres would result in the decline of the cell viability. Especially, only 4.6% of the 4T1 cells could remain alive at the concentration of 200 μg/mL.

4. Conclusions

In summary, we developed a straightforward approach to prepare colloidal PDA/Au hollow spheres by combining mussel-inspired polydopamine chemistry and sacrificial template method, which can be used as multifunctional theranostic agents for simultaneous *in vitro* ultrasound imaging and photothermal therapy. Monodisperse PS spheres were first employed as the template for coating with PDA and subsequently with Au nanoparicles, which were finally removed by trichloromethane, resulting in colloidal PDA/Au hollow spheres. The loading content and size of the Au nanoparticles can be tunable by adjusting the concentration of the Au precursor. This process is facile and green in the absence of toxic chemicals and complicated procedures. To the best of our knowledge, colloidal PDA/Au hollow spheres have not been successfully prepared, especially, for the purpose of simultaneous ultrasound imaging and photothermal therapy of ablating cancer cells. With a proper modification, this approach can be extended as a general preparation strategy for synthesizing composite hollow materials with specified multifunction [31, 43], catering the various demands from practice.

Conflicts of interest

The authors declare no conflicts of interest.

Acknowledgements

We acknowledge the National Natural Science Foundation of China (No.51473089), the Natural Science Basic Research Plan in Shaanxi Province of China (No.2018JM5093), the Program for Science & Technology Innovation Team of Shaanxi Province (No.2018TD-030), the Science and Technology Program of Shaanxi Province (No.2015KJXX-20) and the Fundamental Research Funds for the Central Universities (No.GK201702009, GK201901002) for financial supports. B.P. thank the support from the Academy of Finland (No.321443 and No.328942)

References

[1] E.K. Lim, T. Kim, S. Paik, S. Haam, Y.M. Huh, K. Lee, Nanomaterials for theranostics: Recent advances and future challenges, Chem. Rev. 115 (2015) 327-394.

[2] T. Lammers, S. Aime, W.E. Hennink, G. Storm, F. Kiessling, Theranostic nanomedicine, Acc. Chem. Res. 44 (2011) 1029-1038.

[3] J. Xie, S. Lee, X. Chen, Nanoparticle-based theranostic agents, Adv. Drug Delivery Rev. 62 (2010) 1064-1079.

[4] K. Riehemann, S.W. Schneider, T.A. Luger, B. Godin, M. Ferrari, H. Fuchs, Nanomedicine-challenge and perspectives, Angew. Chem. Int. Ed. 48 (2009) 872-897.

[5] H. Ke, J. Wang, Z. Dai, Y. Jin, E. Qu, Z. Xing, C. Guo, X. Yue, J. Liu, Gold-nanoshelled microcapsules: A theranostic agent for ultrasound contrast imaging and photothermal therapy, Angew. Chem. 123 (2011) 3073-3077.

[6] C. Guo, Y. Jin, Z. Dai, Multifunctional ultrasound contrast agents for imaging guided photothermal therapy, Bioconjug. Chem. 25 (2014) 840-854.

[7] Z. Zha, J. Wang, S. Zhang, S. Wang, E. Qu, Y. Zhang, Z. Dai, Engineering of perfluorooctylbromide polypyrrole nano-/microcapsules for simultaneous contrast enhanced ultrasound imaging and photothermal treatment of cancer, Biomaterials 35 (2014) 287-293.

[8] W.T. Shi, F. Forsberg, Ultrasonic characterization of the nonlinear properties of contrast microbubbles, Ultrasound Med. Biol. 26 (2000) 93-104.

[9] H.R. Herschman, Molecular imaging: Looking at problems, seeing solutions, Science 302 (2003) 605-608.

[10] B.A. Kaufmann, J.R. Lindner, Molecular imaging with targeted contrast ultrasound, Curr. Opin. Biotechnol. 18 (2007) 11-16.

[11] J. Wu, W.L. Nyborg, Ultrasound, cavitation bubbles and their interaction with cells, Adv. Drug Delivery Rev. 60 (2008) 1103-1116.

[12] L.R. Hirsch, R.J. Stafford, J.A. Bankson, S.R. Sershen, B. Rivera, R.E. Price, J.D. Hazle, N.J. Halas, J.L. West, Nanoshell-mediated near-infrared thermal therapy of tumors under magnetic resonance guidance, Proc. Natl. Acad. Sci., 100 (2003) 13549-13554.

[13] H. Ke, J. Wang, Z. Dai, Y. Jin, E. Qu, Z. Xing, C. Guo, J. Liu, X. Yue, Bifunctional gold nanorod-loaded polymeric microcapsules for both contrast-enhanced ultrasound imaging and photothermal therapy, J. Mater. Chem. 21 (2011) 5561-5564.

[14] H. Ke, X. Yue, J. Wang, S. Xing, Q. Zhang, Z. Dai, J. Tian, S. Wang, Y. Jin, Gold nanoshelled liquid perfluorocarbon nanocapsules for combined dual modal ultrasound/CT imaging and photothermal therapy of cancer, Small 10 (2014) 1220-1227.

[15] S. Wang, Z. Dai, H. Ke, E. Qu, X. Qi, K. Zhang, J. Wang, Contrast ultrasound-guided photothermal therapy using gold nanoshelled microcapsules in breast cancer, Eur. J. Radiol. 83 (2014) 117-122.

[16] Z. Zha, J. Wang, E. Qu, S. Zhang, Y. Jin, S. Wang, Z. Dai, Polypyrrole hollow microspheres as echogenic photothermal agent for ultrasound imaging guided tumor ablation, Sci.Rep., 3 (2013) 2360.

[17] X. Jia, X. Cai, Y. Chen, S. Wang, H. Xu, K. Zhang, M. Ma, H. Wu, J. Shi, H. Chen, Perfluoropentane-encapsulated hollow mesoporous prussian blue nanocubes for activated ultrasound imaging and photothermal therapy of cancer, Acs Appl.Mater. Interfaces 7 (2015) 4579-4588.

[18] Y.L. Liu, K.L. Ai, L.H. Lu, Polydopamine and its derivative materials: Synthesis and promising applications in energy, environmental, and biomedical fields, Chem. Rev. 114 (2014) 5057-5115.

[19] H. Lee, S.M. Dellatore, W.M. Miller, P.B. Messersmith, Mussel-inspired surface chemistry for multifunctional coatings, Science 318 (2007) 426-430.

[20] Z. Deng, B. Shang, B. Peng, Polydopamine based colloidal materials: Synthesis and applications, Chem. Rec. 18 (2018) 410-432.

[21] J. Ryu, S.H. Ku, M. Lee, C.B. Park, Bone-like peptide/hydroxyapatite nanocomposites assembled with multi-level hierarchical structures, Soft Matter 7 (2011) 7201-7206.

[22] Y. Xie, J. Wang, Z. Wang, K.A. Krug, J.D. Rinehart, Perfluorocarbon-loaded polydopamine nanoparticles as ultrasound contrast agents, Nanoscale 10 (2018) 12813-12819.

[23] Y. Liu, K. Ai, J. Liu, M. Deng, Y. He, L. Lu, Dopamine-melanin colloidal nanospheres: An efficient near-infrared photothermal therapeutic agent for in vivo cancer therapy, Adv. Mater. 25 (2013) 1353-1359.

[24] J. Wang, Y. Guo, J. Hu, W. Li, Y. Kang, Y. Cao, H. Liu, Development of multifunctional polydopamine nanoparticles as a theranostic nanoplatform against cancer cells, Langmuir 34 (2018) 9516-9524.

[25] X. Huang, I.H. El-Sayed, W. Qian, M.A. El-Sayed, Cancer cell imaging and photothermal therapy in the near-infrared region by using gold nanorods, J. Am. Chem. Soc. 128 (2006) 2115-2120.

[26] P.K. Jain, X. Huang, I.H. El-Sayed, M.A. El-Sayed, Noble metals on the nanoscale: Optical and photothermal properties and some applications in imaging, sensing, biology, and medicine, Acc. Chem. Res. 41 (2008) 1578-1586.

[27] E. Boisselier, D. Astruc, Gold nanoparticles in nanomedicine: Preparations, imaging, diagnostics, therapies and toxicity, Chem. Soc. Rev. 38 (2009) 1759-1782.

[28] Y. Cong, T. Xia, M. Zou, Z. Li, B. Peng, D. Guo, Z. Deng, Mussel-inspired polydopamine coating as a versatile platform for synthesizing polystyrene/Ag nanocomposite particles with enhanced antibacterial activities, J.Mater.Chem.B, 2 (2014) 3450-3461.

[29] Z. Li, C. Wu, K. Zhao, B. Peng, Z. Deng, Polydopamine-assisted synthesis of raspberry-like nanocomposite particles for superhydrophobic and superoleophilic surfaces, Colloid Surf. A., 470 (2015) 80-91.

[30] J. Cui, C. Ma, Z. Li, L. Wu, W. Wei, M. Chen, B. Peng, Z. Deng, Polydopamine-functionalized polymer particles as templates for mineralization of hydroxyapatite: Biomimetic and in vitro bioactivity, RSC Adv., 6 (2016) 6747-6755.

[31] Z.W. Deng, M. Chen, G.X. Gu, L.M. Wu, A facile method to fabricate zno hollow spheres and their photocatalytic property, J. Phys. Chem. B 112 (2008) 16-22.

[32] Y. Wang, B. Shang, M. Liu, F. Shi, B. Peng, Z. Deng, Hollow polydopamine colloidal composite particles: Structure tuning, functionalization and applications, J. Colloid Interface Sci. 513 (2018) 43-52.

[33] C. Wu, G. Zhang, T. Xia, Z. Li, K. Zhao, Z. Deng, D. Guo, B. Peng, Bioinspired synthesis of polydopamine/Ag nanocomposite particles with antibacterial activities, Materials Science and Engineering: C 55 (2015) 155-165.

[34] B. Shang, Y. Wang, P. Yang, B. Peng, Z. Deng, Synthesis of superhydrophobic polydopamine-Ag microbowl/nanoparticle array substrates for highly sensitive, durable and reproducible surface-enhanced raman scattering detection, Sens. Actuat. B: Chem., 255 (2018) 995-1005.

[35] V. Ball, I. Nguyen, M. Haupt, C. Oehr, C. Arnoult, V. Toniazzo, D. Ruch, The reduction of Ag^{+} in metallic silver on pseudomelanin films allows for antibacterial activity but does not imply unpaired electrons, J. Colloid Interface Sci. 364 (2011) 359-365.

[36] D.E. Starr, Z. Liu, M. Haevecker, A. Knop-Gericke, H. Bluhm, Investigation of solid/vapor interfaces using ambient pressure x-ray photoelectron spectroscopy, Chem. Soc. Rev. 42 (2013) 5833-5857.

[37] H. Hu, H. Zhou, J. Du, Z.Q. Wang, L. An, H. Yang, F.H. Li, H.X. Wu, S.P. Yang, Biocompatiable hollow silica microspheres as novel ultrasound contrast agents for in vivo imaging, J. Mater. Chem. 21 (2011) 6576-6583.

[38] L. An, H. Hu, J. Du, J. Wei, L. Wang, H. Yang, D. Wu, H. Shi, F. Li, S. Yang, Paramagnetic hollow silica nanospheres for in vivo targeted ultrasound and magnetic resonance imaging, Biomaterials 35 (2014) 5381-5392.

[39] H. Hu, H. Zhou, J. Liang, L. An, A. Dai, X. Li, H. Yang, S. Yang, H. Wu, Facile synthesis of amino-functionalized hollow silica microspheres and their potential application for ultrasound imaging, J. Colloid Interface Sci. 358 (2011) 392-398.

[40] T. Ye, S. Shun, F. Jiachun, J. Xingguo, Y. Wuli, Mussel-inspired gold hollow superparticles for photothermal therapy, Adv. Healthc. Mater., 4 (2015) 1009-1014.

[41] Z. Yang, J. Ren, Z. Ye, W. Zhu, L. Xiao, L. Zhang, Q. He, Z. Xu, H. Xu, Bio-inspired synthesis of pegylated polypyrrole@polydopamine nanocomposites as theranostic agents for t1-weighted mr imaging guided photothermal therapy, J.Mater.Chem.B, 5 (2017) 1108-1116.

[42] Y. Xiong, F. Sun, Y. Zhang, Z. Yang, P. Liu, Y. Zou, Y. Yu, F. Tong, C. Yi, S. Yang, Z. Xu, Polydopamine-mediated bio-inspired synthesis of copper sulfide nanoparticles for T1-weighted magnetic resonance imaging guided photothermal cancer therapy, Colloid Surf. B., 173 (2019) 607-615.

[43] B. Peng, X. Zhang, D.G.A.L. Aarts, R.P.A. Dullens, Superparamagnetic nickel colloidal nanocrystal clusters with antibacterial activity and bacteria binding ability, Nat. Nanotechnol. 13 (2018) 478-482.

Fig. 1. (a) Schematic diagram illustrating the preparation of colloidal PDA/Au hollow spheres; Transmission electron microscopy (TEM) images of (b) colloidal PS spheres; (c) colloidal PS/PDA composite spheres; (d) colloidal PS/PDA/Au composite spheres; (e) colloidal PDA/Au

hollow spheres. (f) Energy-dispersive X-ray spectroscopy (EDX) analysis of PDA/Au hollow sphere. Scale bars are applicable to all images in the row. (g) X-ray photoelectron spectroscopy (XPS) measurements and (h) X-ray diffraction (XRD) patterns of the samples shown in (b-e).

Fig. 2. TEM images of colloidal PDA/Au hollow spheres prepared by varying the concentrations of $HAuCl_4$: (a) 0.10 mg/mL, PDA/Au-i; (b) 0.17 mg/mL, PDA/Au-ii, and (c) 0.33 mg/mL, PDA/Au-iii. (d, e and f) The size distribution histograms and corresponding normal fittings of Au nanoparticles shown in (a), (b), and (c), respectively. (g) XRD patterns and (h) TGA curves of the samples shown in (a-c).

Fig. 3. *In vitro* ultrasound images of colloidal PDA/Au hollow spheres (PDA/Au-i, PDA/Au-ii, PDA/Au-iii, respectively). (MI: 0.06, Frequency: 9 MHz, the concentration of PDA/Au hollow spheres: 0.04, 0.06, 0.08, 0.10, 0.20 mg/mL).

Fig. 4. (a) UV-vis-NIR spectra of colloidal PDA hollow spheres and colloidal PDA/Au hollow spheres in aqueous solution. (b) Temperature elevation of colloidal PDA hollow spheres and PDA/Au hollow spheres at same concentration (200 μg/mL) under 808 nm NIR laser irradiation. (c) Temperature elevation of colloidal PDA/Au hollow spheres at different concentrations under 808 nm NIR laser irradiation. Note that PBS buffer was used as the blank in both (b) and (c). (d) Photothermal response of colloidal PDA/Au hollow spheres in aqueous solution (200 μg/mL) under irradiation for 900 s and then turning off the irradiation (Insert: the linear time data versus $-ln\theta$ obtained from the cooling period). 808 nm NIR laser with 1 W/cm^2 and PDA/Au-iii were used throughout all experiments.

Fig. 5. Fluorescence images of 4T1 breast cancer cell lines incubation with colloidal PDA/Au hollow spheres (100 μg/mL) at 37 ^oC for 1 h (a) before and (b) after the laser irradiation (808 nm, 1 W/cm^2 for 10 min). The cells were stained with calcein AM (live cells, green fluorescence) and

PI (dead cells, red fluorescence), respectively. (c) Cell viability of 4T1 cells after incubation with increased concentrations of colloidal PDA/Au hollow spheres in the absence of irradiation. (d) Cell viability of 4T1 cells treated with different concentrations of colloidal PDA/Au hollow spheres after laser irradiation (808 nm, 1 W/cm^2 for 10 min).

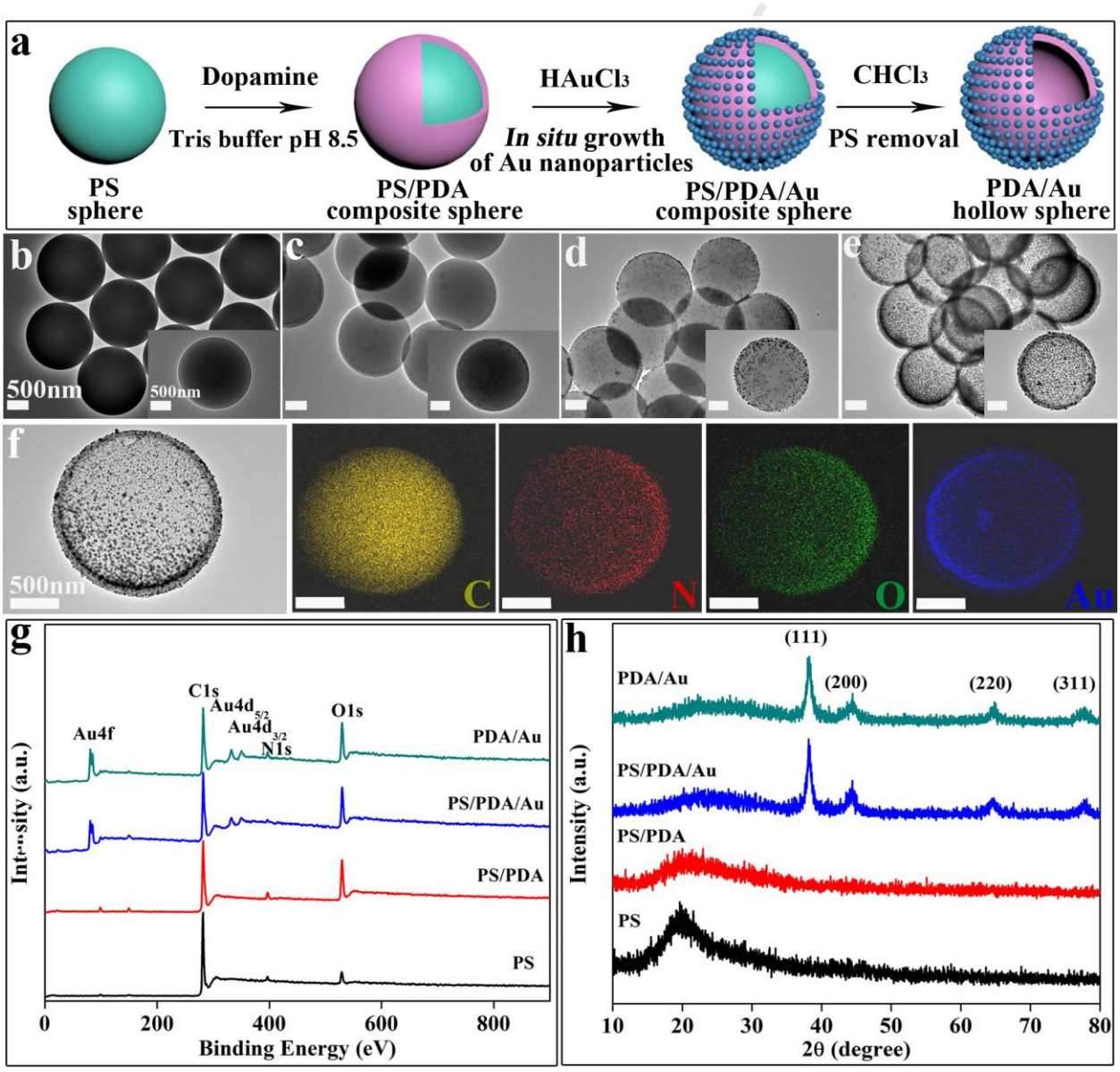

Fig. 1. (a) Schematic diagram illustrating the preparation of colloidal PDA/Au hollow spheres; Transmission electron microscopy (TEM) images of (b) colloidal PS spheres; (c) colloidal PS/PDA composite spheres; (d) colloidal PS/PDA/Au composite spheres; (e) colloidal PDA/Au hollow spheres. (f) Energy-dispersive X-ray spectroscopy (EDX) analysis of PDA/Au hollow sphere. Scale bars are applicable to all images in the row. (g) X-ray photoelectron spectroscopy (XPS) measurements and (h) X-ray diffraction (XRD) patterns of the samples shown in (b-e).

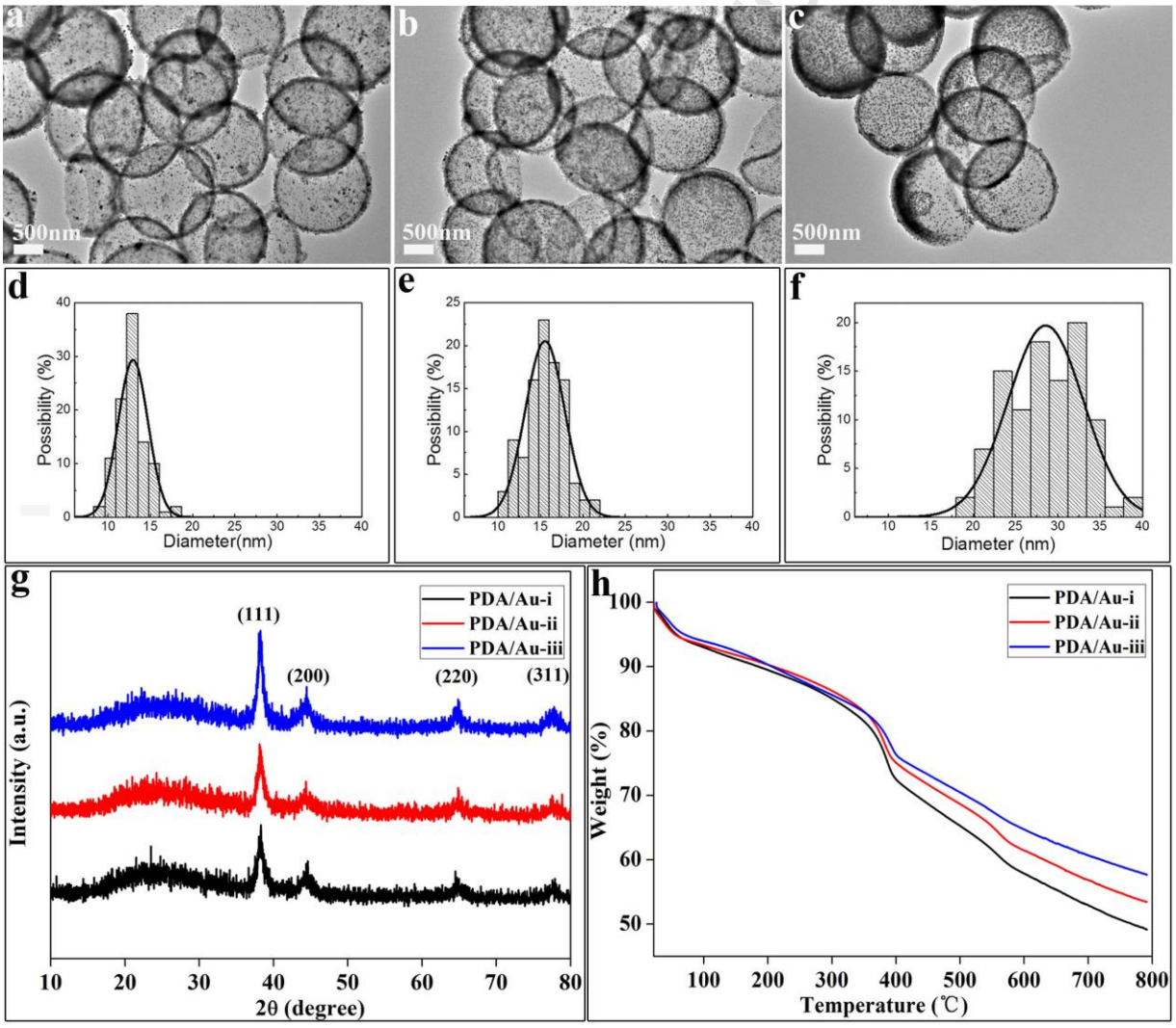

Fig. 2. TEM images of colloidal PDA/Au hollow spheres prepared by varying the concentrations of $HAuCl_4$: (a) 0.10 mg/mL, PDA/Au-i; (b) 0.17 mg/mL, PDA/Au-ii, and (c) 0.33 mg/mL, PDA/Au-iii. (d, e and f) The size distribution histograms and corresponding normal fittings of Au nanoparticles shown in (a), (b), and (c), respectively. (g) XRD patterns and (h) TGA curves of the samples shown in (a-c).

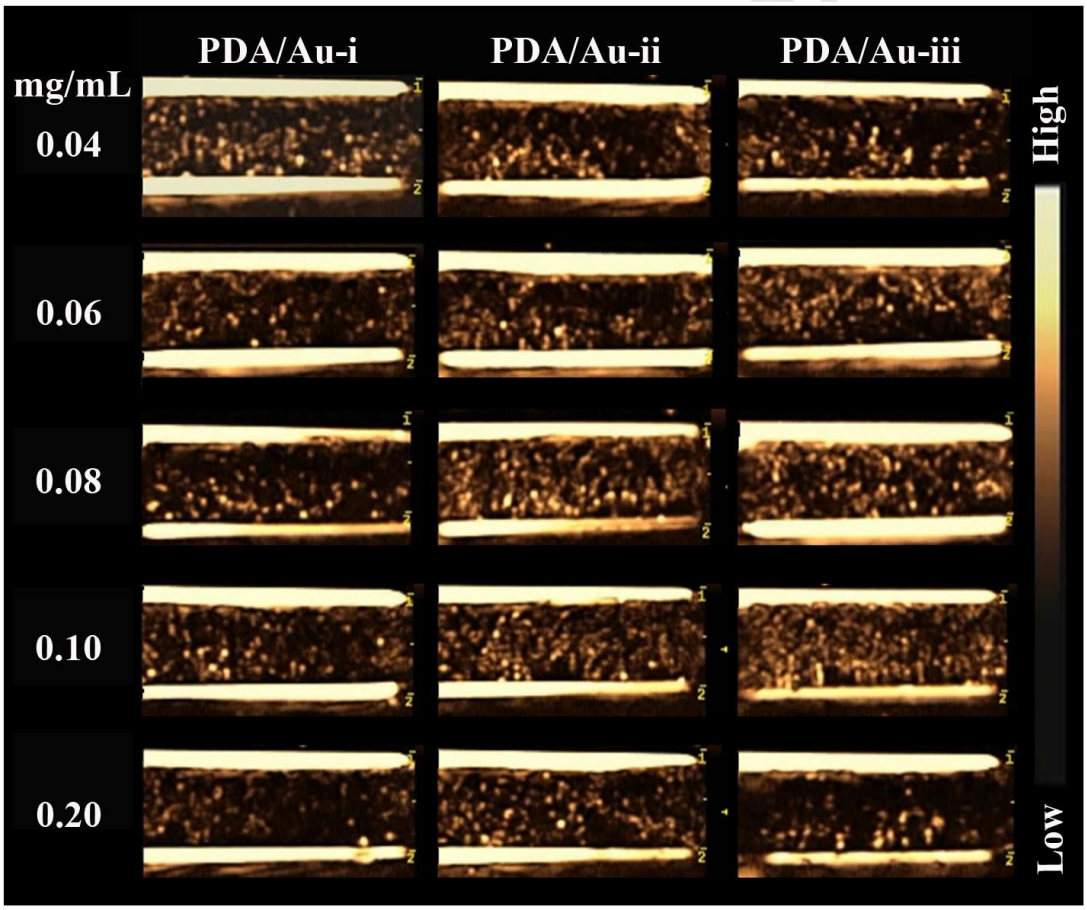

Fig. 3. *In vitro* ultrasound images of colloidal PDA/Au hollow spheres (PDA/Au-i, PDA/Au-ii, PDA/Au-iii, respectively). (MI: 0.06, Frequency: 9 MHz, the concentration of PDA/Au hollow spheres: 0.04, 0.06, 0.08, 0.10, 0.20 mg/mL).

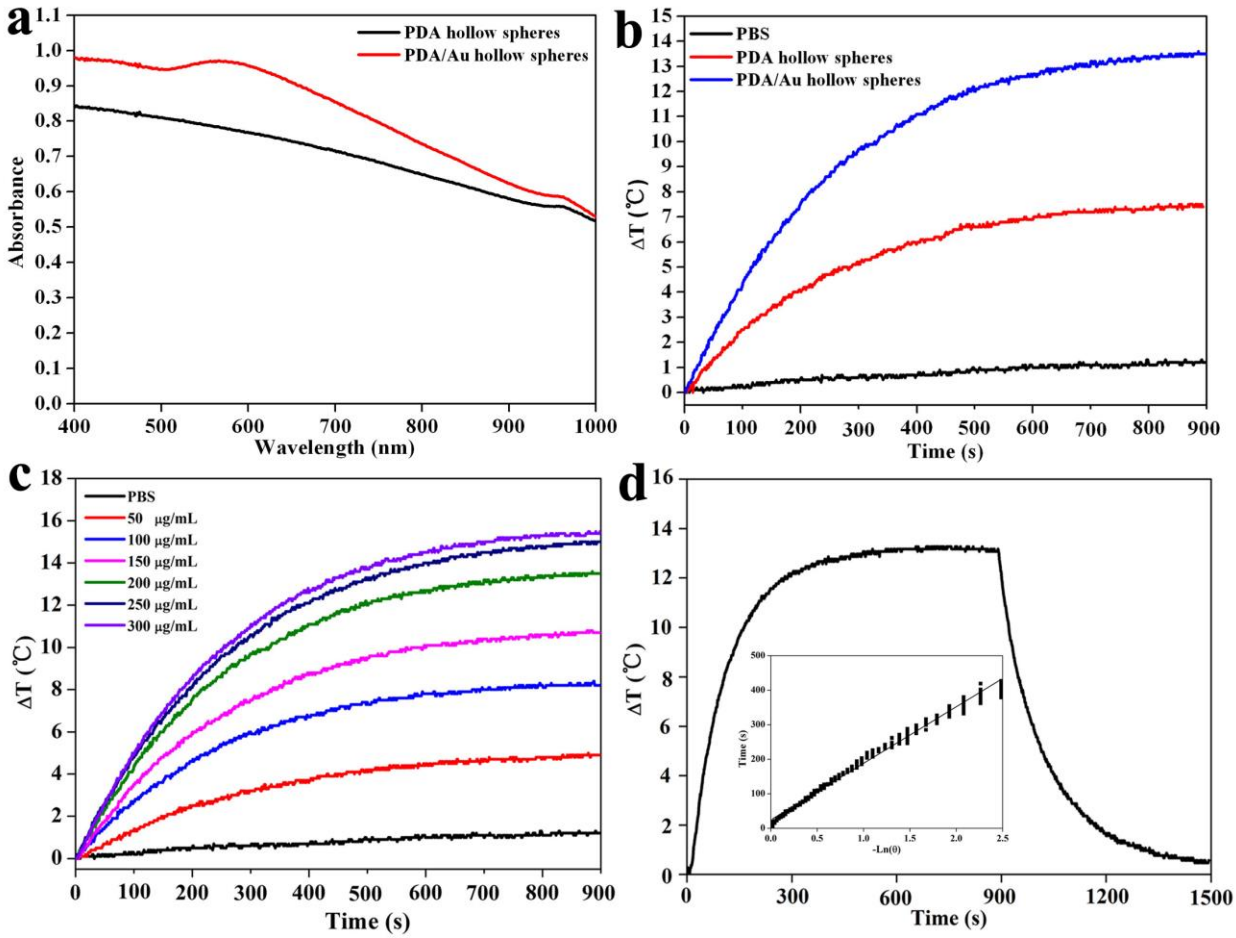

Fig. 4. (a) UV-vis-NIR spectra of colloidal PDA hollow spheres and colloidal PDA/Au hollow spheres in aqueous solution. (b) Temperature elevation of colloidal PDA hollow spheres and PDA/Au hollow spheres at same concentration (200 μg/mL) under 808 nm NIR laser irradiation. (c) Temperature elevation of colloidal PDA/Au hollow spheres at different concentrations under 808 nm NIR laser irradiation. Note that PBS buffer was used as the blank in both (b) and (c). (d) Photothermal response of colloidal PDA/Au hollow spheres in aqueous solution (200 μg/mL) under irradiation for 900 s and then turning off the irradiation (Insert: the linear time data versus $-ln\theta$ obtained from the cooling period). 808 nm NIR laser with 1 W/cm^2 and PDA/Au-iii were used throughout all experiments.

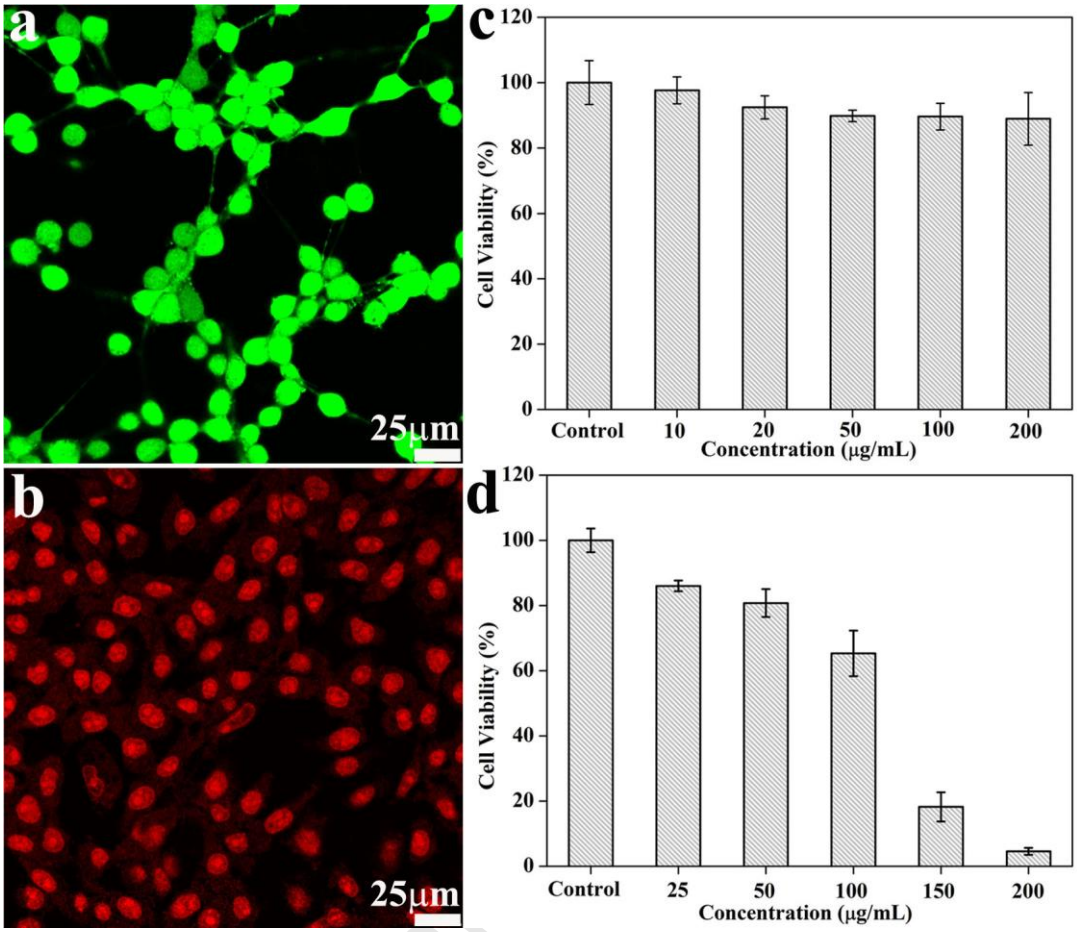

Fig. 5. Fluorescence images of 4T1 breast cancer cell lines incubation with colloidal PDA/Au hollow spheres (100 μg/mL) at 37 ^{o}C for 1 h (a) before and (b) after the laser irradiation (808 nm, 1 W/cm^2 for 10 min). The cells were stained with calcein AM (live cells, green fluorescence) and PI (dead cells, red fluorescence), respectively. (c) Cell viability of 4T1 cells after incubation with increased concentrations of colloidal PDA/Au hollow spheres in the absence of irradiation. (d) Cell viability of 4T1 cells treated with different concentrations of colloidal PDA/Au hollow spheres after laser irradiation (808 nm, 1 W/cm^2 for 10 min).

Graphical Abstract

Colloidal polydopamine/Au (PDA/Au) hollow spheres fabricated via polydopamine chemistry combing with sacrificial template method, can serve as theranostic agents for *in vitro* ultrasound imaging and photothermal therapy.

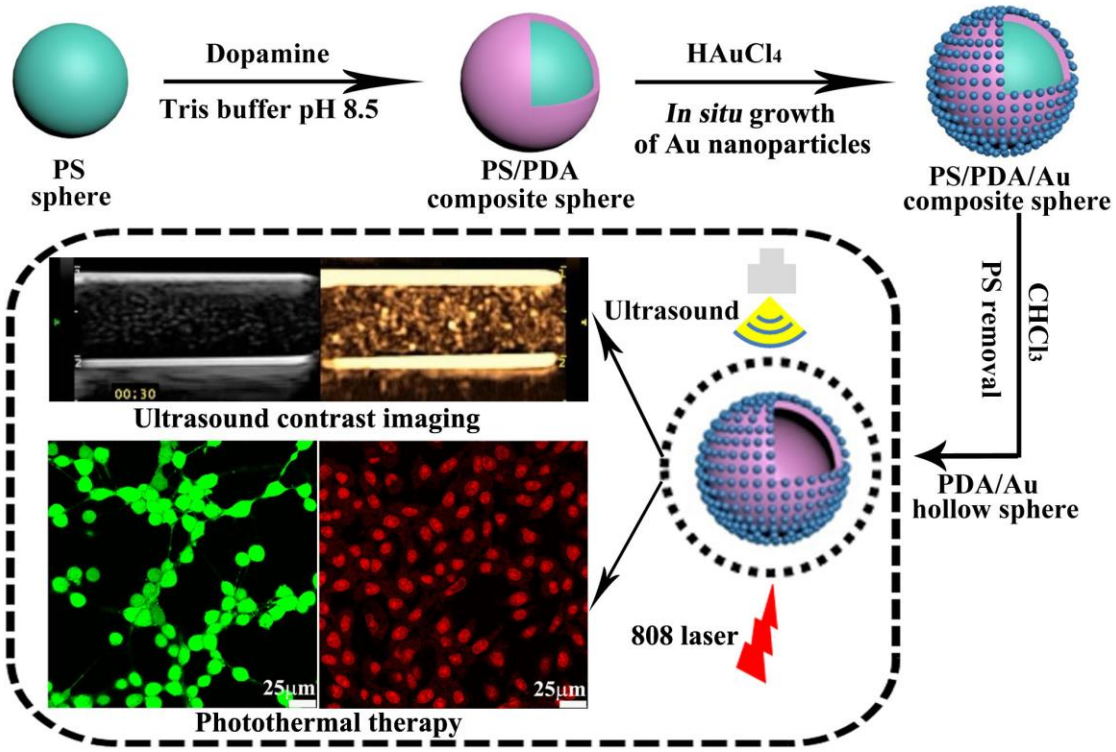

Highlights

- Polydopamine/Au (PDA/Au) hollow spheres were prepared by combining mussel-inspired polydopamine chemistry with sacrificial template method.
- PDA/Au hollow spheres showed a fine cytocompatibility.
- PDA/Au hollow spheres can serve as theranostic agents for *in vitro* ultrasound imaging and photothermal therapy